1

Nanospray desorption electrospray ionization (nano-DESI) mass

spectrometry imaging with high ion mobility resolution

Li-Xue Jiang¹, Emerson Hernly¹, Hang Hu¹, Ryan T. Hilger¹, Heiko Neuweger², Manxi Yang¹,

Julia Laskin¹*

¹Department of Chemistry, Purdue University, West Lafayette, IN, 47907, United States

²Bruker Daltonics GmbH & Co. KG, Bremen, 28359, Germany

*Corresponding author

E-mail: ilaskin@purdue.edu

Abstract

Untargeted separation of isomeric and isobaric species in mass spectrometry imaging (MSI) is

challenging. The combination of ion mobility spectrometry (IMS) with MSI has emerged as an

effective strategy for differentiating isomeric and isobaric species, which substantially enhances

the molecular coverage and specificity of MSI experiments. In this study, we have implemented

nanospray desorption electrospray ionization (nano-DESI) MSI on a trapped ion mobility

spectrometry (TIMS) mass spectrometer. A new nano-DESI source was constructed, and a

specially designed inlet extension was fabricated to accommodate the new source. The nano-DESI-

TIMS-MSI platform was evaluated by imaging mouse brain tissue sections. We achieved high ion

mobility resolution by utilizing three narrow mobility scan windows that cover the majority of the

lipid molecules. Notably, the mobility resolution reaching up to 300 in this study is much higher

than the resolution obtained in our previous study using drift tube IMS. High-resolution TIMS

successfully separated lipid isomers and isobars revealing their distinct localizations in tissue

samples. Our results further demonstrate the power of high mobility resolution IMS for unraveling

the complexity of biomolecular mixtures analyzed in MSI experiments.

Keywords: Mass spectrometry imaging; Trapped ion mobility spectrometry (TIMS); Nanospray desorption electrospray ionization (nano-DESI); Lipid isomers; High mobility resolution

I. Introduction

Mass spectrometry imaging (MSI) is a powerful analytical technique used to study the localization of many classes of molecules including metabolites, glycans, lipids, peptides, and proteins in biological systems. ^{1–10} Over the past two decades, advances in spatial resolution have enabled MSI to distinguish cellular structures. ¹¹ Concurrently, the speed of MSI has increased by 1-2 orders of magnitude. ¹² A majority of MSI experiments are performed using high-resolution mass spectrometers that efficiently separate isobaric species. ¹³ Alternatively, tandem mass spectrometry (MS/MS)-based MSI approaches have been used to examine the spatial localization of both isomers and isobars in a targeted manner. ^{14–17} Despite these impressive developments, the untargeted separation of isomeric species in MSI is challenging, which complicates data interpretation and limits the molecular specificity of the technique.

Ion mobility spectrometry (IMS) is a gas-phase technique that separates ions based on their collision cross section (CCS) with a background gas. 18-22 In IMS, the separation is achieved on a timescale of tens of milliseconds, which makes it ideally suited for coupling with MSI techniques. ^{23,24} Coupling of IMS with MSI reduces spectral complexity, eliminates overlaps with background peaks, and enables differentiation of isobaric and isomeric species thereby substantially enhancing molecular coverage and specificity of MSI experiments. Furthermore, CCS measurements facilitate the identification of molecules extracted from different locations on the sample. Drift tube ion mobility spectrometry (DTIMS)²⁵ and traveling wave ion mobility spectrometry (TWIMS)²⁶ have been successfully coupled with several MSI techniques including matrix-assisted laser desorption/ionization (MALDI),²⁷ desorption electrospray ionization (DESI), ^{28–30} nanospray desorption electrospray ionization (nano-DESI), ^{31,32} laser ablation electrospray ionization (LAESI),^{33,34} liquid extraction surface analysis (LESA),³⁵ and infrared matrix-assisted laser desorption electrospray ionization (IR-MALDESI).³⁶ Recently, MALDI MSI has been performed on a trapped ion mobility spectrometry (TIMS)³⁷ and its high mobility resolution capabilities have been highlighted.^{38–41} In one study, isobaric lipid species at m/z 782.561 separated by TIMS using the mobility resolution of about 100 showed distinct localizations in muscle tissue and oocytes of a female gammarid. 40 In another study, three lipid isomers with distinct spatial distributions were observed in a whole-body mouse pup tissue section.³⁸

In this study, we use TIMS to enhance the molecular specificity of nano-DESI MSI. Nano-DESI is an ambient ionization technique that uses a dynamic liquid bridge formed by a specially designed probe for localized extraction of molecules from a sample. 42-44 The extracted analyte mixture is transferred to a mass spectrometer inlet and ionized by electrospray ionization. Internal standards are added to the extraction solvent to ensure accurate relative quantification in nano-DESI MSI experiments. Recent developments of nano-DESI MSI instrumentation have enabled imaging with high spatial resolution and high throughput. 45-48 Furthermore, we have developed approaches for improving the extraction and ionization efficiency of analytes by tailoring the composition of the extraction solvent. 49,50 These efforts have enhanced the sensitivity and depth of molecular coverage of the technique. However, similar to other MSI techniques, nano-DESI relies on the simultaneous analysis of hundreds of extracted species, many of which cannot be separated using high-resolution mass spectrometry. To address this challenge, we have previously coupled DTIMS separation with nano-DESI MSI and obtained isomer-selective ion images of several lipids.³¹ Although some isomeric species could be identified based on the shapes of ion mobility peaks, the resolution of DTIMS of ~60 was insufficient to obtain a clear separation of lipid isomers. In contrast, TIMS provides access to a higher mobility resolution of >200 and >300 for singly and multiply charged ions, respectively. 51-53 In this study, we implemented nano-DESI MSI on a timsTOF Pro2 mass spectrometer and used the high mobility resolution of this system to examine the localization of lipid isomers and closely spaced isobaric species in tissues using mouse brain as a model system.

2. Methods

2.1 Chemicals and materials

HPLC grade water and LC-MS grade methanol were purchased from Acros Organics (NJ). Lysophosphatidylcholine 17:1 (LPC 17:1); Phosphatidylcholine 18:2 (Cis) (DLPC) (PC 18:2) and 18:1 (11-cis) (PC 18:1); phosphocholine 12:0-13:0 (PC 12:0-13:0) were obtained from Avanti Polar Lipids (Alabaster, AL). Supelco stainless-steel tubes with an outer diameter of 1/16 in. were acquired from MilliporeSigma. The ESI-L low concentration tune mix (G1969-85000, Agilent Technologies, CA) was used to calibrate the instrument.

2.2 Tissue preparation

Fresh frozen C57BL/6 mouse brain tissues were purchased from BioIVT (Westbury, NY). Tissues were sectioned axially to a thickness of 12 μ m at a temperature of -21 °C using a CM1850 Cryostat (Leica Microsystems, Wetzlar, Germany) and thaw-mounted onto glass microscope slides (IMEB, Inc Tek-Select Gold Series Microscope Slides, Clear Glass, Positive Charged). All sections were stored in a -80 °C freezer prior nano-DESI MSI analysis.

2.3 Coupling of nano-DESI to timsTOF

A new nano-DESI source was designed and coupled to a timsTOF Pro2 mass spectrometer (Bruker Daltonics, Bremen, Germany), as shown in **Figure 1a**. The source design is similar to our previously reported nano-DESI sources.³¹ Briefly, a tissue section on a glass slide is mounted onto an XYZ stage, which is composed of three motorized stages from Zaber Technologies Inc. (Vancouver, Canada). The X motorized stage has a long travel distance of 500 mm, which was selected for future applications. Meanwhile, the Y and Z stages are the same as in our previous designs. The nano-DESI probe (**Figure 1b**) and shear force probe are positioned using micropositioners (XYZ500-TIM) from Quater Research & Development (Bend, OR). The shear force probe contains two piezo plates and is used to control the distance between the sample and the nano-DESI probe. Two Dino-Lite digital microscopes (model AM7115MZTL, Dino-Lite, Torrance, CA) are used to facilitate the setup and monitor the liquid bridge during MSI experiments. The imaging platform is controlled by custom-designed LabVIEW software (National Instruments, Austin, TX).

To couple the nano-DESI source, the commercial ESI source was removed from the timsTOF instrument, and the inlet was modified to incorporate an extension necessary to accommodate the new source. **Figure 1c** shows the design of the MS inlet extension. A custom-designed capillary cap is used to hold a 50 mm-long stainless steel tube with an inner diameter of 0.5 mm, which serves as the extension. The cap is in an electrical contact with the heated inlet of the instrument, which ensures that the high voltage is applied to the extension tube. To ensure good vacuum suction through the extension tube, an O-ring is used to seal it against the heated capillary. A custom-designed endplate is used to press the O-ring and align the entire assembly.

MSI data were acquired in lines using Compass HyStar 6.2 (Bruker Daltonics GmbH & Co. KG, Bremen) software by scanning the sample under the nano-DESI probe. The instrument acquisition

was triggered using a contact closure signal supplied to the data acquisition computer through an RS232 connector. The acquisition time was selected to match the time of the individual line scan. The instrument method was optimized to maximize the signal and resolution.

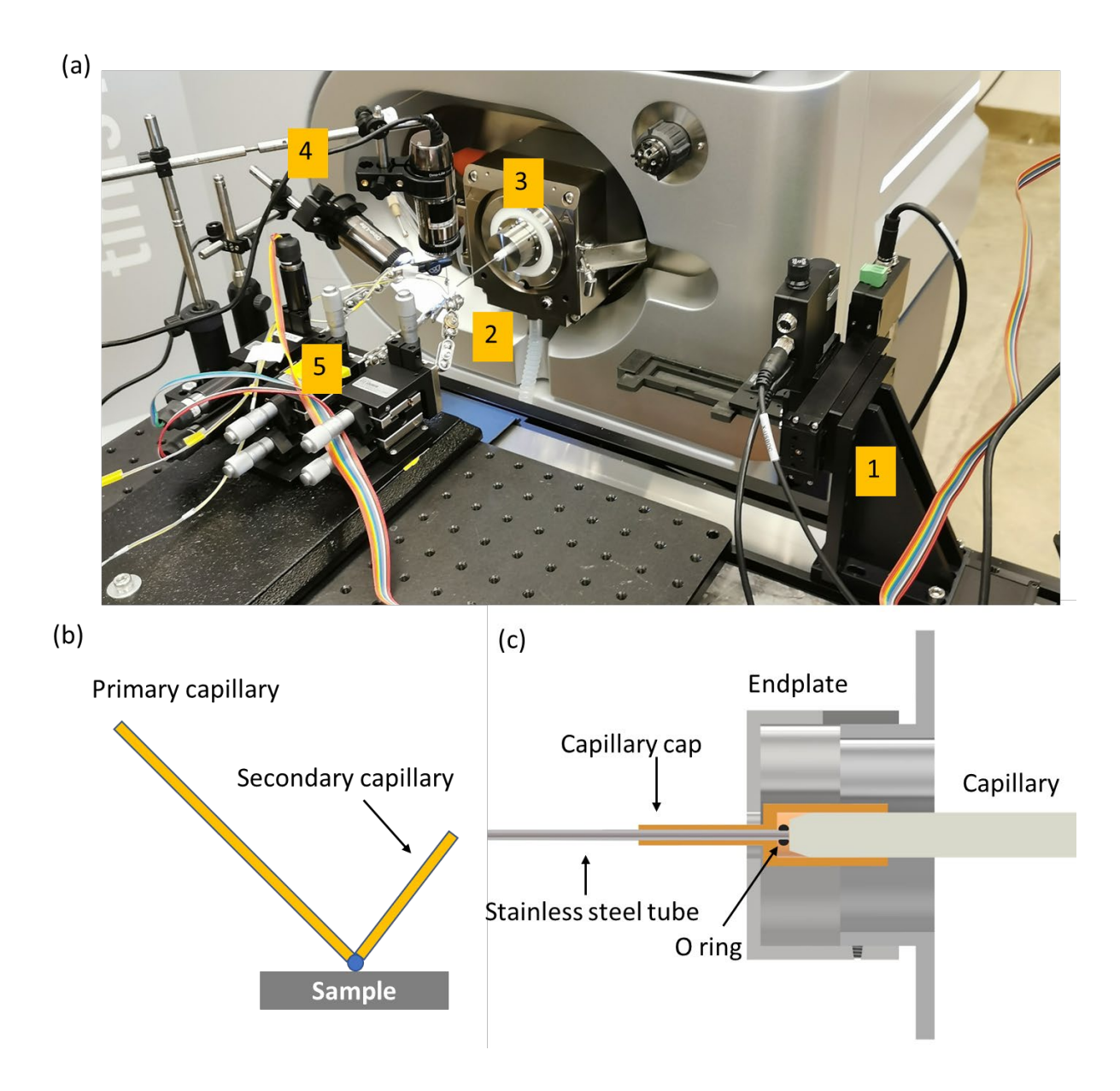


Figure 1. (a) A photograph of the nano-DESI source coupled to a timsTOF instrument. (1) XYZ stage; (2) Nanospray capillary; (3) Capillary extension; (4) Dino-Lite microscope; (5) Micropositioners. (b) A schematic drawing of the nano-DESI probe. (c) A schematic drawing of the extension tube attached to the timsTOF inlet for coupling with the nano-DESI source.

2.4 Nano-DESI timsTOF MSI

Two fused silica capillaries (50 μ m ID, 150 μ m OD, Polymicro Technologies L.L.C., Phoenix, AZ) were used to form the nano-DESI probe. The primary capillary is connected to a syringe filled with the extraction solvent, 1 μ M PC 12:0-13:0 in 9:1 MeOH:H₂O (v/v). The extraction solvent is propelled through the primary capillary at a flow rate of 0.5 μ L/min using the syringe pump of the timsTOF instrument. A liquid bridge is formed between the probe and the sample surface when they get close to each other. The extracted analytes are continuously transferred and analyzed by the timsTOF mass spectrometer. A continuous line scan mode, in which mass spectra are acquired while the sample is moved under the probe in lines, is used in nano-DESI MSI experiments. A 3-point method was used to control the distance between the nano-DESI probe and the sample surface. The mobility was calibrated in the reduced mobility (1/ K_0) range of 1.18-1.39 with a ramp time of 940 ms using the ESI-L low concentration tune mix. The mobility scan range for MSI was set as 1.30-1.51 with the same ramp time of 940 ms. The accumulation time was 100 ms. A high voltage of -4 kV was applied to the inlet to obtain a stable Taylor cone. The dry gas temperature was set at 300 °C. The line scan rate was 100 μ m/s and the step between lines was 250 μ m.

For the MSI experiments performed in the high mobility resolution mode, three narrow mobility scan windows: 1.38-1.43, 1.42-1.47, and 1.46-1.51 were used in alternating line scans. The accumulation time was 200 ms and the ramp time for each scan window was 993 ms, corresponding to a data acquisition rate of 1 Hz per scan window. The mobility was calibrated using two phosphatidylcholine standards: PC 18:2 and PC 18:1. Only one mobility window was calibrated and the other two windows were used without calibration because the instrument cannot carry multiple calibration information. To minimize the mobility drift during MSI, the "Tunnel In Vacuum" pressure was maintained in the range of 2.503-2.513 mBar by manually adjusting the source gas flow valve. The flow rate of extraction solvent was $0.7 \,\mu\text{L/min}$. The line scan rate was $80 \,\mu\text{m/s}$ and the step between lines was $60 \,\mu\text{m}$.

2.5 Data Analysis

Each line scan was acquired as an individual file (.d file format). Data processing was performed using a custom-designed Python code, which was modified to incorporate the new data format

(https://github.com/LabLaskin/MSI-image-generator). For tims-off data, the raw data is stored in two files: analysis.tsf which contains all instrument parameters and meta information for both the analysis and each acquired mass spectrum, and analysis.tsf bin which contains the respective binary representations of the acquired mobility, mass-to-charge, and intensity information. Analysis.tsf is an SQLite database, which is accessed through sqlite3 module in Python. Analysis.tsf bin is a compressed binary form, which is accessible through timsdata.dll from Bruker. The timsdata.dll exports a simple C-language API for Python. Every mass spectrum in the line scan is treated as a single pixel. Ion images are constructed by plotting the abundance of a list of targeted m/z features in each mass spectrum (pixel) within the mass tolerance window of ± 25 ppm as a function of the location on the tissue. Ion signals are normalized either to the signal of the internal standard or total ion count (TIC). Tims-on data is accessed through Alphatims⁵⁴ and processed in a similar fashion. The mobility tolerance window is determined by the experimental settings. For nano-DESI timsTOF MSI experiments, the mobility for each pixel was corrected based on the "Tunnel In Vacuum" pressure. Candidate assignments of the observed m/z features were obtained by searching against LIPID MAPS (www.lipidmaps.org); final assignments are based on the MS/MS analysis.

3. Results and Discussion

In this study, we implemented nano-DESI MSI on a timsTOF instrument and used the high ion mobility resolution mode to perform isomer-selective imaging of lipids in biological tissues. A stainless-steel extension tube was designed and attached to the heated inlet of the timsTOF system as shown in **Figure 1c.** The design of the extension, in which a capillary tube is inserted into a holder and sealed against the inlet allowed us to test ion transfer efficiency of extension tubes with different diameters and lengths. We used ESI to evaluate the performance of different extension tubes. In these experiments, the ESI-L low concentration tune mix was delivered to the inlet through a fused silica capillary at a flow rate of $0.4 \mu L/min$ and ionized by applying -4 kV to the instrument inlet. Mass spectra were acquired after optimizing the position of the capillary relative to the extension tube. Stainless steel tubes with an inner diameter (I.D.) of 1.0, 0.75, and 0.5 mm were tested. Signals of the peak at m/z 1221.99 obtained for different lengths and diameters of the extension tube are summarized in **Figure S1**. These results indicate that the transmission efficiency

increases with a decrease in the length and I.D. of the extension tube with the best signal obtained using a 50 mm-long I.D. 0.5 mm tube. This tube was subsequently used in all the nano-DESI MSI experiments. Mass spectra of the tune mix with and without the extension tube are shown in **Figure S2**. The two spectra look very similar with a slightly lower signal obtained in the presence of the extension tube.

A mouse brain tissue section was used to evaluate the performance of nano-DESI MSI on the timsTOF instrument. We used a mobility scan range of 1.30-1.51 with a ramp time of 940 ms to examine lipids extracted from the tissue. Most of the abundant lipids are in the m/z range of 750–880 and mobility range of 1.37-1.50. Representative positive mode mobility-selected ion images of lipids in mouse brain tissue are shown in **Figure 2a**. This experiment was performed using mobility resolution of up to 200, as shown in **Figure S3**. This mobility resolution enables the separation of the majority of isobaric and some isomeric lipids as previously reported in MALDI TIMS MSI experiments.^{39,41} However, some lipid isomers and isobars cannot be separated. **Figure 2b** shows the mobilogram of m/z 770.51 \pm 0.02 obtained using the mobility resolution of 200, in which three poorly-separated mobility peaks were found.

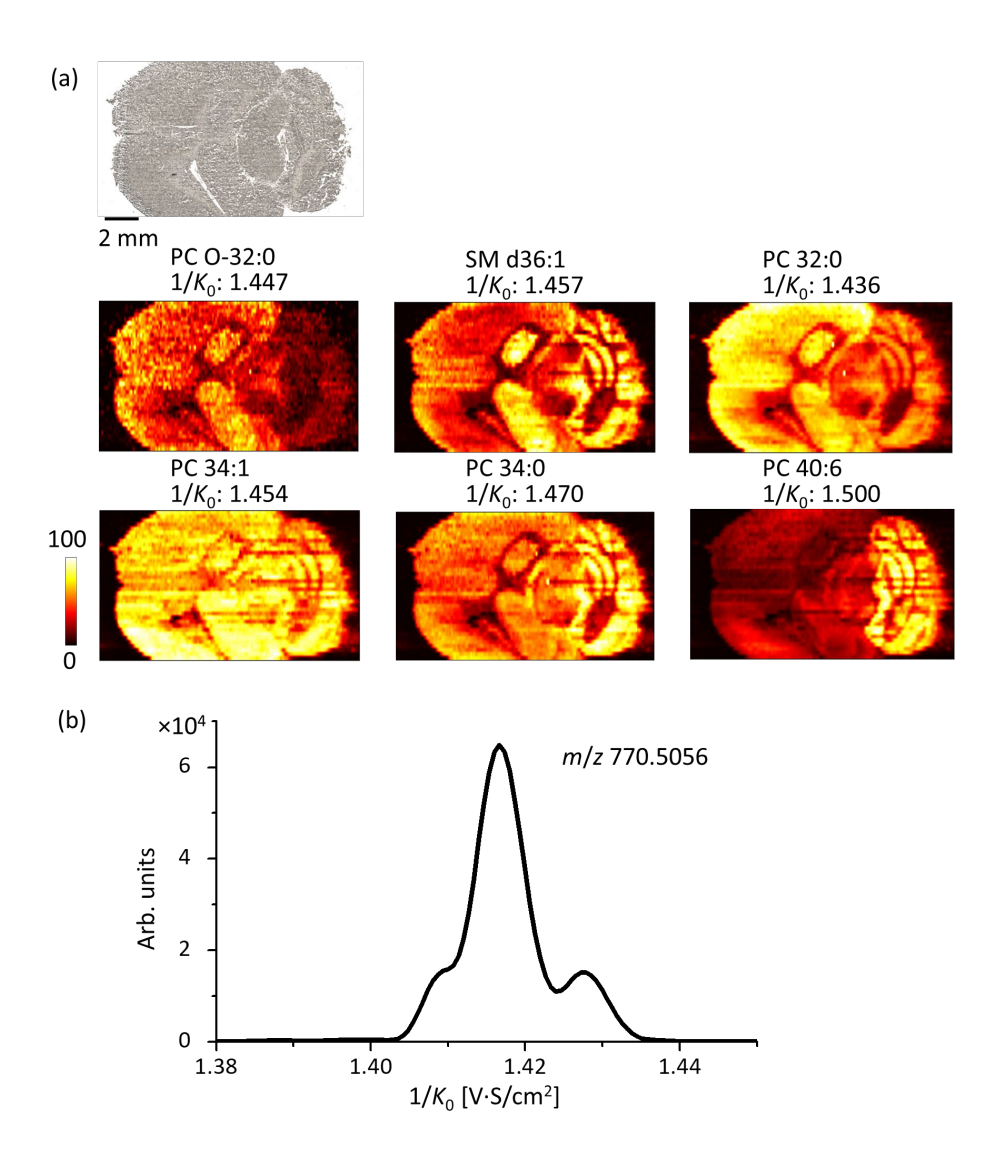


Figure 2. (a) Optical image and representative positive mode mobility-selected ion images of $[M+K]^+$ ions of phospholipids in mouse brain tissue obtained using nano-DESI MSI on timsTOF. Scale bar: 2 mm; the intensity scale: black (low), yellow (high). The experimental parameters are as follows: scan rate of 100 µm/s, step between lines 250 µm, accumulation time of 100 ms, ramp time for each scan window of 940 ms. Ion images are normalized to TIC. (b) Extracted ion mobilogram of m/z 770.51 \pm 0.02. The mobility tolerance window is \pm 0.004.

To achieve higher mobility resolution in MSI using TIMS, we used narrow mobility scan windows and longer ramp scan times. Herein, three mobility scan windows of 1.38-1.43, 1.42-1.47, and 1.46-1.51 in alternating line scans were used to explore the localization of lipids over the m/z range

of 700-900 in another mouse brain tissue section. A small overlap between the mobility scan windows was selected to ensure adequate detection of lipid species with mobilities at the edge of the scan windows. Each line scan was acquired using only one mobility scan window. The step size between adjacent lines was 60 µm, resulting in a 180 µm line spacing between the lines acquired for each mobility scan window. After the acquisition, line scans obtained for the same mobility scan window were grouped and processed together to generate ion images. We found that mobility drifted slightly during the MSI experiment. This drift has little or no effect when a wide mobility scan window is used, but it cannot be ignored for narrow mobility scan windows. To alleviate this problem, the "Tunnel In Vacuum" pressure was kept in a certain range through manually adjusting the source gas flow valve. During visualization, the mobility for each pixel was corrected based on the "Tunnel In Vacuum" pressure. Representative positive mode mobility-selected ion images of molecules in mouse brain tissue from the three scan windows are shown in **Figure 3**. Most of the lipids were observed in the scan window of 1.42-1.47.

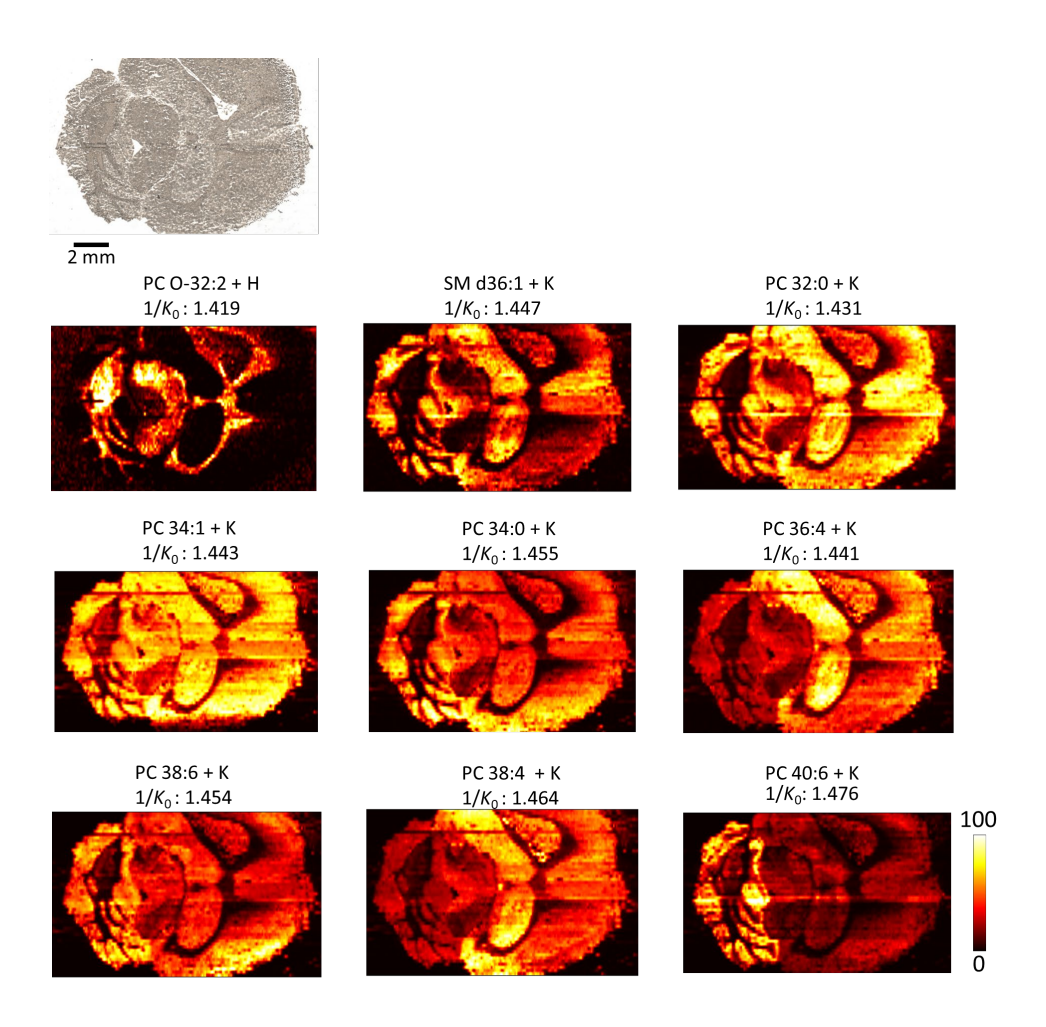


Figure 3. Optical image and representative positive mode mobility-selected ion images of phospholipids in mouse brain tissue obtained using nano-DESI MSI on tims TOF. Scale bar: 2 mm; the intensity scale: black (low), yellow (high). The experimental parameters are as follows: scan rate of 80 μ m/s, step between lines for the same mobility scan window of 180 μ m, accumulation time of 200 ms, ramp time for each scan window of 993 ms. Ion images are normalized to TIC. The mobility tolerance window is ± 0.003 .

The mobility resolution of up to 300 was achieved in these experiments as shown in **Figure S4**. This high mobility resolution is key to resolving lipid isomers. In the mobility scan window of 1.38-1.43, three isomers were found at m/z 770.5077. **Figure 4a** shows the heatmap obtained for a small region of the mass spectrum averaged over one line scan. In the heat map, a red line observed at m/z 770.5077 implies that there are several species with the same m/z. The extracted ion mobilogram of m/z of 770.51 \pm 0.02 shown in **Figure 4b** contains three distinct peaks. Ion

images shown in **Figure 4c** correspond to the sum of all of the features observed at *m/z*: 770.5077 in the mobility range of 1.406-1.430 and three separate ion images for features in mobility ranges of 1.406-1.412, 1.414-1.419, and 1.422-1.428. The three separate ion images show distinct distributions. Because the peaks at mobility of 1.410 and 1.416 show similar abundance, the ion image obtained over the wide mobility window is a combination of the two peaks. The species with mobility of 1.410 is more abundant in the hippocampal region. Meanwhile, the peak with mobility of 1.424 is low in abundance in the cerebellum region. According to the accurate mass and MS/MS data (**Figure S5**), the mobility peak centered at 1.410 was assigned as [PE O-38:7 + Na]⁺. The mobility peaks centered at 1.416 and 1.424 were assigned as two isomers of [PC 32:1 + K]⁺. The individual fatty acid chain lengths could not be identified based on the MS/MS data. Additional ion images of isomeric species that are well separated in mobility are provided in **Figure S6**, which demonstrates the advantage of high mobility resolution.

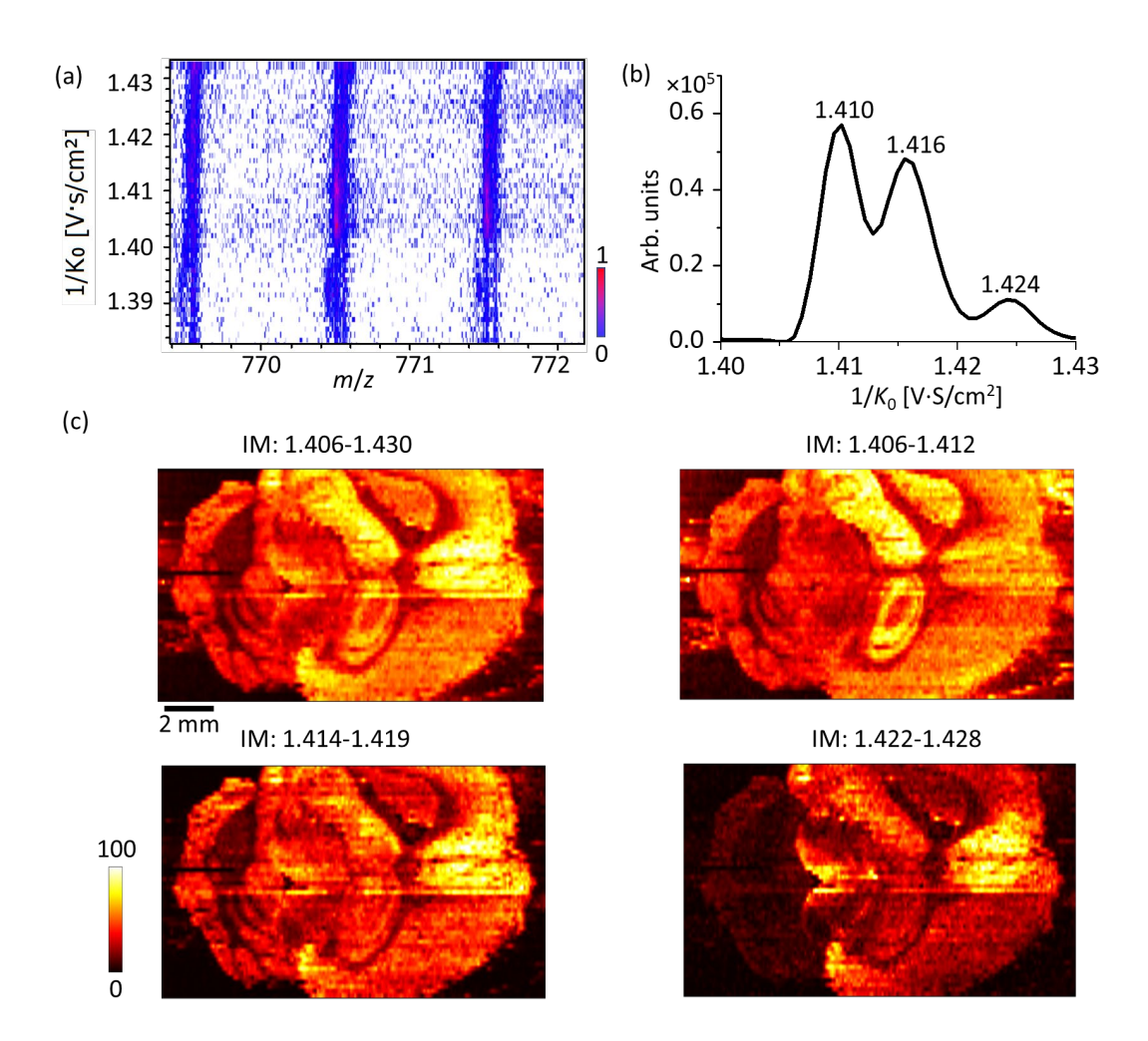


Figure 4. (a) A heatmap of a narrow m/z range of a mass spectrum averaged over a line scan; (b) Extracted ion mobilogram of m/z 770.51 \pm 0.02; (c) Ion images of m/z 770.5077 extracted over four mobility ranges. The optical image of the mouse brain tissue section is the same as that in Figure 3.

In addition to isomer-selective imaging, coupling of nano-DESI MSI with TIMS is advantageous for separating isobars, which is critical to obtaining ion images free of interferences. Isobars are common in MSI experiments focused on imaging of lipids in tissues. Isobars originate from the complexity of the lipid mixture extracted from a tissue sample and formation of multiple adducts of lipids. In this study, we found that high mobility resolution enables separation of some isobaric species that cannot be distinguished based on their m/z. For example, the extracted ion mobilogram of the peak of m/z of 798.54 ± 0.02 , one of the most abundant lipid signals in mouse brain nano-

DESI MSI experiments, shown in Figure 5a is asymmetric indicating the presence of overlapping features. Fitting of the mobilogram with a sum of two Gaussian peaks shown in Figure 5a adequately describes the observed peak shape. Although the two peaks centered at 1.439 and 1.443 are not fully separated in ion mobility, ion images extracted for mobility ranges of 1.434-1.439 and 1.443-1.450, in which only one of the peaks is dominant, show distinct distributions (Figure 5d and 5e). A fractional distribution image was obtained by plotting the abundance ratio of the signal obtained for the 1.439 mobility peak over the total signal of both peaks (Figure 5f). The relative abundance of peak 1.439 is increased in the white matter. Meanwhile, the mobility peak at 1.443 is abundant in the grey matter. The sum image generated over a broader mobility range of 1.434-1.450 that includes both peaks shows an almost uniform distribution across the tissue indicating the importance of high-resolution mobility separation for obtaining accurate localization of some of the lipid species. The mobility peak at 1.443 was assigned as [PC 34:1 + K]+ with a theoretical m/z of 798.5410, while the mobility peak of 1.439 was assigned as [PE O-40:7 + Na]⁺ with a theoretical m/z of 798.5408. The MS/MS mass spectra are shown in Figure S7. A mass resolving power of 4 million, which is inaccessible on most commercial mass spectrometers, is required to separate these two closely spaced isobars. Additional ion images of isomeric and isobaric species that cannot be fully separated in mobility are provided in Figure S8. They all show distinct distributions over the mouse brain tissue. Our results demonstrate the advantages of high-resolution TIMS separation coupled with nano-DESI MSI and highlight some challenges. In particular, some lipids cannot be separated using the highest mobility resolution accessible using timsTOF. In addition, the trade-off between mobility resolution and mobility range presents a challenge to using this system in a discovery mode. Nevertheless, our results demonstrate the power of ion mobility separation for unraveling the complexity of lipid mixtures extracted from biological tissues in nano-DESI MSI experiments.

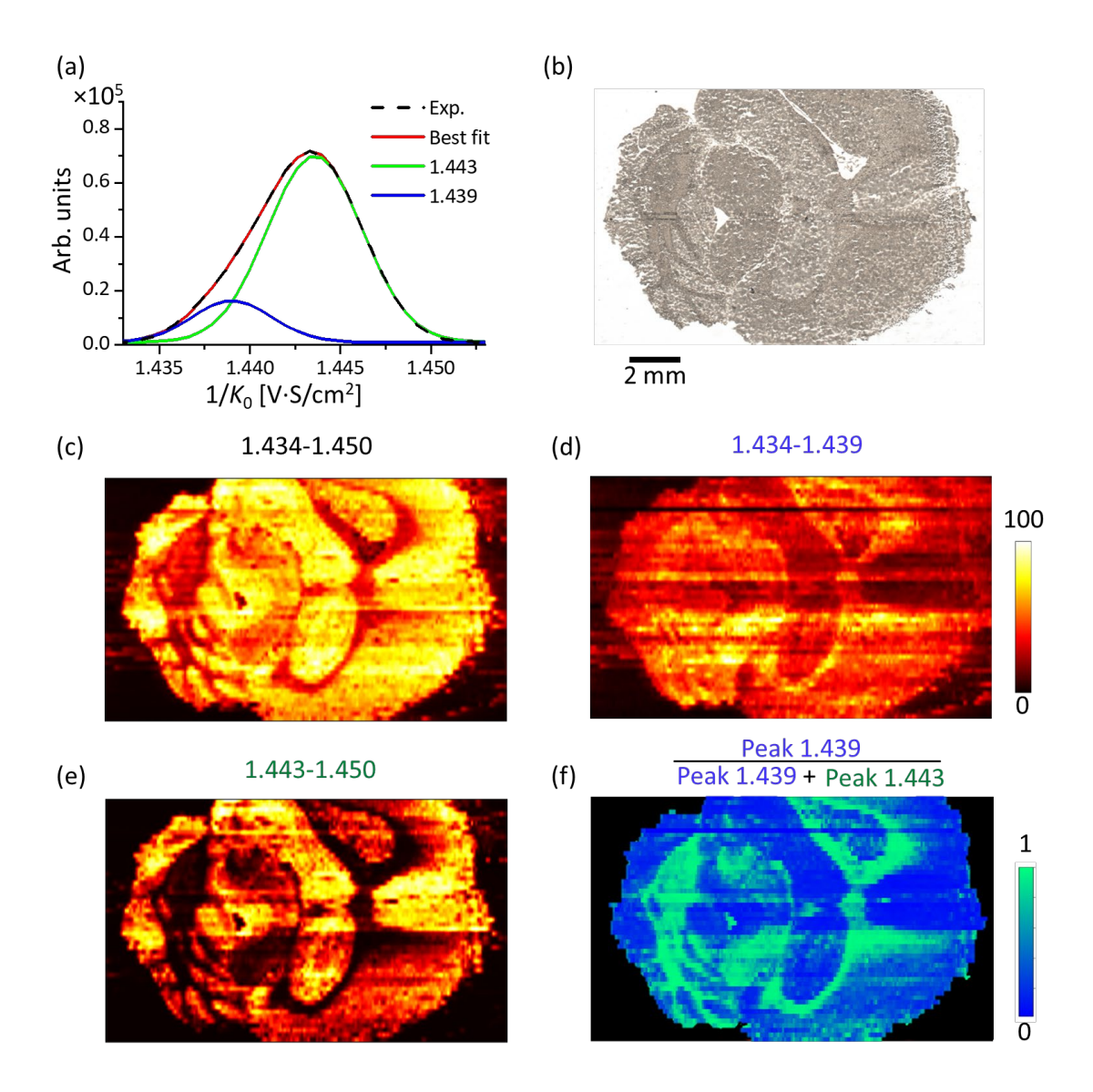


Figure 5. (a) The experimental mobilogram of m/z 798.54 \pm 0.02 (dashed line) and the result obtained by fitting the experimental curve with a sum of two Gaussian peaks (solid red line). The individual Gaussian peaks centered at 1.439 and 1.443 are shown as green and blue lines, respectively. (b) The optical image of mouse brain tissue section. (c) A composite ion image generated for the mobility range of 1.434-1.450. Ion images of the two isobaric peaks averaged over mobility ranges of 1.434-1.439 (d) and 1.443-1.450 (e). (f) A fractional distribution image showing that the relative abundance of the mobility peak centered at 1.439 is increased in the white matter region.

4. Conclusions

IMS is a gas phase separation technique that holds great promise for the separation of both isobaric and isomeric biomolecules extracted from biological tissues in MSI experiments. Nevertheless, the resolution of some IMS platforms is insufficient for separating isomeric lipids. To overcome this limitation, we have successfully implemented nano-DESI MSI on a timsTOF instrument that offers high ion mobility resolution. A new nano-DESI source was constructed and a specially designed inlet extension was fabricated to accommodate the new source. The extension was optimized to ensure good ion transmission from the nano-DESI source to the timsTOF inlet. The nano-DESI-TIMS-MSI experiment was evaluated using mouse brain tissue sections. The acquisition method that enables ion mobility separation with high resolution during MSI uses three narrow mobility scan windows to cover most of the lipid molecules. The mobility resolution of up to 300 achieved in this study is much higher than the resolution obtained in our previous study using DTIMS. Lipid isomers and isobars showing distinct localizations in tissue samples have been separated by TIMS, demonstrating the advantage of high mobility resolution in MSI experiments.

Supporting Information

Supporting Information is available free of charge on the ACS Publications website.

Mass spectra showing the performance of the extension tube, extracted mobilogram showing the ion mobility resolution, MS/MS mass spectra, and additional ion images of isomeric and isobaric molecules (PDF)

Acknowledgements

The authors acknowledge support from the National Institutes of Health (NIH) Award RF1MH128866 (BICCN) and UH3CA255132 (HuBMAP) along with support from the National Science Foundation (NSF-2108729). The authors thank Dr. Savannah Snyder and Dr. Xuejun Peng from Bruker Daltonics for technical support and helpful discussions.

References

- (1) Buchberger, A. R.; DeLaney, K.; Johnson, J.; Li, L. Mass Spectrometry Imaging: A Review of Emerging Advancements and Future Insights. *Anal Chem* **2018**, *90* (1), 240–265. https://doi.org/10.1021/ACS.ANALCHEM.7B04733.
- (2) Norris, J. L.; Caprioli, R. M. Analysis of Tissue Specimens by Matrix-Assisted Laser Desorption/Ionization Imaging Mass Spectrometry in Biological and Clinical Research. *Chem Rev* **2013**, *113* (4), 2309–2342. https://doi.org/10.1021/CR3004295.
- (3) McDonnell, L. A.; Heeren, R. M. A. Imaging Mass Spectrometry. *Mass Spectrom Rev* **2007**, *26* (4), 606–643. https://doi.org/10.1002/MAS.20124.
- (4) Swales, J. G.; Hamm, G.; Clench, M. R.; Goodwin, R. J. A. Mass Spectrometry Imaging and Its Application in Pharmaceutical Research and Development: A Concise Review. *Int J Mass Spectrom* **2019**, *437*, 99–112. https://doi.org/10.1016/j.ijms.2018.02.007.
- (5) Schulz, S.; Becker, M.; Groseclose, M. R.; Schadt, S.; Hopf, C. Advanced MALDI Mass Spectrometry Imaging in Pharmaceutical Research and Drug Development. *Curr Opin Biotechnol* **2019**, *55*, 51–59. https://doi.org/10.1016/J.COPBIO.2018.08.003.
- (6) Xiao, Y.; Deng, J.; Yao, Y.; Fang, L.; Yang, Y.; Luan, T. Recent Advances of Ambient Mass Spectrometry Imaging for Biological Tissues: A Review. *Anal Chim Acta* **2020**, 1117, 74–88. https://doi.org/10.1016/J.ACA.2020.01.052.
- (7) Perez, C. J.; Bagga, A. K.; Prova, S. S.; Yousefi Taemeh, M.; Ifa, D. R. Review and Perspectives on the Applications of Mass Spectrometry Imaging under Ambient Conditions. *Rapid Communications in Mass Spectrometry* **2019**, *33* (S3), 27–53. https://doi.org/10.1002/RCM.8145.
- (8) Zhao, C.; Cai, Z. Three-Dimensional Quantitative Mass Spectrometry Imaging in Complex System: From Subcellular to Whole Organism. *Mass Spectrom Rev* **2022**, *41* (3), 469–487. https://doi.org/10.1002/MAS.21674.
- (9) Baker, T. C.; Han, J.; Borchers, C. H. Recent Advancements in Matrix-Assisted Laser Desorption/Ionization Mass Spectrometry Imaging. *Current Opinion in Biotechnology*. Elsevier Ltd February 1, 2017, pp 62–69. https://doi.org/10.1016/j.copbio.2016.09.003.
- (10) Unsihuay, D.; Sanchez, D. M.; Laskin, J. Quantitative Mass Spectrometry Imaging of Biological Systems. *Annu Rev Phys Chem* **2020**, *72*, 307–329. https://doi.org/10.1146/annurev-physchem-061020-053416.
- (11) Ma, S.; Leng, Y.; Li, X.; Meng, Y.; Yin, Z.; Hang, W. High Spatial Resolution Mass Spectrometry Imaging for Spatial: Advances, Challenges, and Future Perspectives. *TRAC*-

- TRENDS IN ANALYTICAL CHEMISTRY **2023**, 159. https://doi.org/10.1016/j.trac.2022.116902.
- (12) Jiang, L. X.; Yang, M.; Wali, S. N.; Laskin, J. High-Throughput Mass Spectrometry Imaging of Biological Systems: Current Approaches and Future Directions. *TrAC Trends* in Analytical Chemistry 2023, 163, 117055. https://doi.org/10.1016/J.TRAC.2023.117055.
- (13) Römpp, A.; Spengler, B. Mass Spectrometry Imaging with High Resolution in Mass and Space. *Histochemistry and Cell Biology*. June 2013, pp 759–783. https://doi.org/10.1007/s00418-013-1097-6.
- (14) Guo, X. Y.; Cao, W. B.; Fan, X. M.; Guo, Z. Y.; Zhang, D. H.; Zhang, H. Y.; Ma, X. X.; Dong, J. H.; Wang, Y. F.; Zhang, W. P.; Ouyang, Z. Tandem Mass Spectrometry Imaging Enables High Definition for Mapping Lipids in Tissues. *ANGEWANDTE CHEMIE-INTERNATIONAL EDITION*. https://doi.org/10.1002/anie.202214804.
- (15) Prentice, B. M.; Chumbley, C. W.; Caprioli, R. M. High-Speed MALDI MS/MS Imaging Mass Spectrometry Using Continuous Raster Sampling. *JOURNAL OF MASS SPECTROMETRY* **2015**, *50* (4), 703–710. https://doi.org/10.1002/jms.3579.
- (16) Prentice, B. M.; Chumbley, C. W.; Caprioli, R. M. Absolute Quantification of Rifampicin by MALDI Imaging Mass Spectrometry Using Multiple TOF/TOF Events in a Single Laser Shot. *J Am Soc Mass Spectrom* **2017**, *28* (1), 136–144. https://doi.org/10.1007/s13361-016-1501-2.
- (17) Lanekoff, I.; Burnum-Johnson, K.; Thomas, M.; Short, J.; Carson, J. P.; Cha, J.; Dey, S. K.; Yang, P.; Prieto Conaway, M. C.; Laskin, J. High-Speed Tandem Mass Spectrometric in Situ Imaging by Nanospray Desorption Electrospray Ionization Mass Spectrometry. *Anal Chem* 2013, 85 (20), 9596–9603. https://doi.org/10.1021/ac401760s.
- (18) Dodds, J. N.; Baker, E. S. Ion Mobility Spectrometry: Fundamental Concepts, Instrumentation, Applications, and the Road Ahead. *J Am Soc Mass Spectrom* **2019**, *30* (11), 2185–2195. https://doi.org/10.1007/s13361-019-02288-2.
- (19) Paglia, G.; Smith, A. J.; Astarita, G. Ion Mobility Mass Spectrometry in the Omics Era: Challenges and Opportunities for Metabolomics and Lipidomics. *Mass Spectrom Rev* **2022**, *41* (5), 722–765. https://doi.org/10.1002/mas.21686.
- (20) Kanu, A. B.; Dwivedi, P.; Tam, M.; Matz, L.; Hill Jr., H. H. Ion Mobility-Mass Spectrometry. *Journal of Mass Spectrometry* **2008**, *43* (1), 1–22. https://doi.org/10.1002/JMS.1383.
- (21) Burnum-Johnson, K. E.; Baker, E. S.; Metz, T. O. Characterizing the Lipid and Metabolite Changes Associated with Placental Function and Pregnancy Complications Using Ion

- Mobility Spectrometry-Mass Spectrometry and Mass Spectrometry Imaging. *Placenta* **2017**, *60*, S67–S72. https://doi.org/10.1016/J.PLACENTA.2017.03.016.
- (22) Burnum-Johnson, K. E.; Zheng, X.; Dodds, J. N.; Ash, J.; Fourches, D.; Nicora, C. D.; Wendler, J. P.; Metz, T. O.; Waters, K. M.; Jansson, J. K.; Smith, R. D.; Baker, E. S. Ion Mobility Spectrometry and the Omics: Distinguishing Isomers, Molecular Classes and Contaminant Ions in Complex Samples. *TrAC Trends in Analytical Chemistry* **2019**, *116*, 292–299. https://doi.org/10.1016/J.TRAC.2019.04.022.
- (23) Rivera, E. S.; Djambazova, K. V.; Neumann, E. K.; Caprioli, R. M.; Spraggins, J. M. Integrating Ion Mobility and Imaging Mass Spectrometry for Comprehensive Analysis of Biological Tissues: A Brief Review and Perspective. *Journal of Mass Spectrometry* **2020**, 55 (12). https://doi.org/10.1002/JMS.4614.
- (24) Sans, M.; Feider, C. L.; Eberlin, L. S. Advances in Mass Spectrometry Imaging Coupled to Ion Mobility Spectrometry for Enhanced Imaging of Biological Tissues. *Curr Opin Chem Biol* **2018**, *42*, 138–146. https://doi.org/10.1016/J.CBPA.2017.12.005.
- (25) Cohen, M. J.; Karasek, F. W. Plasma Chromatographytm -a New Dimension for Gas Chromatography and Mass Spectrometry. *J Chromatogr Sci* **1970**, *8* (6), 330–337. https://doi.org/10.1093/CHROMSCI/8.6.330.
- (26) Giles, K.; Pringle, S. D.; Worthington, K. R.; Little, D.; Wildgoose, J. L.; Bateman, R. H. Applications of a Travelling Wave-Based Radio-Frequency-Only Stacked Ring Ion Guide. *Rapid Communications in Mass Spectrometry* **2004**, *18* (20), 2401–2414. https://doi.org/10.1002/RCM.1641.
- (27) McLean, J. A.; Ridenour, W. B.; Caprioli, R. M. Profiling and Imaging of Tissues by Imaging Ion Mobility-Mass Spectrometry. *Journal of Mass Spectrometry* **2007**, *42* (8), 1099–1105. https://doi.org/10.1002/JMS.1254.
- (28) Guo, R.; Zhou, L.; Chen, X. Desorption Electrospray Ionization (DESI) Source Coupling Ion Mobility Mass Spectrometry for Imaging Fluoropezil (DC20) Distribution in Rat Brain. *Anal Bioanal Chem* **2021**, *413* (23), 5835–5847. https://doi.org/10.1007/s00216-021-03563-6.
- (29) Hou, J.; Zhang, Z.; Zhang, L.; Wu, W.; Huang, Y.; Jia, Z.; Zhou, L.; Gao, L.; Long, H.; Lei, M.; Wu, W.; Guo, D. Spatial Lipidomics of Eight Edible Nuts by Desorption Electrospray Ionization with Ion Mobility Mass Spectrometry Imaging. *Food Chem* **2022**, *371*. https://doi.org/10.1016/J.FOODCHEM.2021.130893.
- (30) Towers, M. W.; Karancsi, T.; Jones, E. A.; Pringle, S. D.; Claude, E. Optimised Desorption Electrospray Ionisation Mass Spectrometry Imaging (DESI-MSI) for the Analysis of Proteins/Peptides Directly from Tissue Sections on a Travelling Wave Ion

- Mobility Q-ToF. *J Am Soc Mass Spectrom* **2018**, *29* (12), 2456–2466. https://doi.org/10.1007/S13361-018-2049-0.
- (31) Unsihuay, D.; Yin, R.; Sanchez, D. M.; Yang, M.; Li, Y.; Sun, X.; Dey, S. K.; Laskin, J. High-Resolution Imaging and Identification of Biomolecules Using Nano-DESI Coupled to Ion Mobility Spectrometry. *Anal Chim Acta* 2021, 1186, 339085. https://doi.org/10.1016/J.ACA.2021.339085.
- (32) Hale, O. J.; Hughes, J. W.; Cooper, H. J. Simultaneous Spatial, Conformational, and Mass Analysis of Intact Proteins and Protein Assemblies by Nano-DESI Travelling Wave Ion Mobility Mass Spectrometry Imaging. *Int J Mass Spectrom* **2021**, *468*. https://doi.org/10.1016/J.IJMS.2021.116656.
- (33) Li, H.; Smith, B. K.; Márk, L.; Nemes, P.; Nazarian, J.; Vertes, A. Ambient Molecular Imaging by Laser Ablation Electrospray Ionization Mass Spectrometry with Ion Mobility Separation. *Int J Mass Spectrom* **2015**, *377* (1), 681–689. https://doi.org/10.1016/J.IJMS.2014.06.025.
- (34) Li, H.; Balan, P.; Vertes, A. Molecular Imaging of Growth, Metabolism, and Antibiotic Inhibition in Bacterial Colonies by Laser Ablation Electrospray Ionization Mass Spectrometry. *Angewandte Chemie International Edition* **2016**, *55* (48), 15035–15039. https://doi.org/10.1002/ANIE.201607751.
- (35) Griffiths, R. L.; Sisley, E. K.; Lopez-Clavijo, A. F.; Simmonds, A. L.; Styles, I. B.; Cooper, H. J. Native Mass Spectrometry Imaging of Intact Proteins and Protein Complexes in Thin Tissue Sections. *Int J Mass Spectrom* **2019**, *437*, 23–29. https://doi.org/10.1016/J.IJMS.2017.10.009.
- (36) Ekelöf, M.; Dodds, J.; Khodjaniyazova, S.; Garrard, K. P.; Baker, E. S.; Muddiman, D. C. Coupling IR-MALDESI with Drift Tube Ion Mobility-Mass Spectrometry for High-Throughput Screening and Imaging Applications. *J Am Soc Mass Spectrom* **2020**, *31* (3), 642–650. https://doi.org/10.1021/jasms.9b00081.
- (37) Fernandez-Lima, F.; Kaplan, D. A.; Suetering, J.; Park, M. A. Gas-Phase Separation Using a Trapped Ion Mobility Spectrometer. *International Journal for Ion Mobility Spectrometry* **2011**, *14* (2), 93–98. https://doi.org/10.1007/S12127-011-0067-8.
- (38) Djambazova, K. V.; Dufresne, M.; Migas, L. G.; Kruse, A. R. S.; Van de Plas, R.; Caprioli, R. M.; Spraggins, J. M. MALDI TIMS IMS of Disialoganglioside Isomers—GD1a and GD1b in Murine Brain Tissue. *Anal Chem* **2022**, *95* (2), 1176–1183. https://doi.org/10.1021/acs.analchem.2c03939.
- (39) Spraggins, J. M.; Djambazova, K. V; Rivera, E. S.; Migas, L. G.; Neumann, E. K.; Fuetterer, A.; Suetering, J.; Goedecke, N.; Ly, A.; Van de Plas, R.; Caprioli, R. M. High-

- Performance Molecular Imaging with MALDI Trapped Ion-Mobility Time-of-Flight (TimsTOF) Mass Spectrometry. *Anal Chem* **2019**, *91* (22), 14552–14560. https://doi.org/10.1021/acs.analchem.9b03612.
- (40) Fu, T.; Oetjen, J.; Chapelle, M.; Verdu, A.; Szesny, M.; Chaumot, A.; Degli-Esposti, D.; Geffard, O.; Clément, Y.; Salvador, A.; Ayciriex, S. In Situ Isobaric Lipid Mapping by MALDI–Ion Mobility Separation–Mass Spectrometry Imaging. *Journal of Mass Spectrometry* **2020**, *55* (9), e4531. https://doi.org/10.1002/JMS.4531.
- (41) Djambazova, K. V.; Klein, D. R.; Migas, L. G.; Neumann, E. K.; Rivera, E. S.; Van de Plas, R.; Caprioli, R. M.; Spraggins, J. M. Resolving the Complexity of Spatial Lipidomics Using MALDI TIMS Imaging Mass Spectrometry. *Anal Chem* **2020**, *92* (19), 13290–13297. https://doi.org/10.1021/acs.analchem.0c02520.
- (42) Roach, P. J.; Laskin, J.; Laskin, A. Nanospray Desorption Electrospray Ionization: An Ambient Method for Liquid-Extraction Surface Sampling in Mass Spectrometry. *Analyst* **2010**, *135* (9), 2233–2236. https://doi.org/10.1039/C0AN00312C.
- (43) Laskin, J.; Heath, B. S.; Roach, P. J.; Cazares, L.; Semmes, O. J. Tissue Imaging Using Nanospray Desorption Electrospray Ionization Mass Spectrometry. *Anal Chem* **2012**, *84* (1), 141–148. https://doi.org/10.1021/ac2021322.
- (44) Duncan, K. D.; Bergman, H. M.; Lanekoff, I. A Pneumatically Assisted Nanospray Desorption Electrospray Ionization Source for Increased Solvent Versatility and Enhanced Metabolite Detection from Tissue. *Analyst* 2017, 142 (18), 3424–3431. https://doi.org/10.1039/C7AN00901A.
- (45) Yin, R.; Burnum-Johnson, K. E.; Sun, X.; Dey, S. K.; Laskin, J. High Spatial Resolution Imaging of Biological Tissues Using Nanospray Desorption Electrospray Ionization Mass Spectrometry. *Nat Protoc* **2019**, *14* (12), 3445–3470. https://doi.org/10.1038/s41596-019-0237-4.
- (46) Li, X.; Hu, H.; Yin, R.; Li, Y.; Sun, X.; Dey, S. K.; Laskin, J. High-Throughput Nano-DESI Mass Spectrometry Imaging of Biological Tissues Using an Integrated Microfluidic Probe. *Anal Chem* **2022**, *94* (27), 9690–9696. https://doi.org/10.1021/acs.analchem.2c01093.
- (47) Yang, M.; Unsihuay, D.; Hu, H.; Nguele Meke, F.; Qu, Z.; Zhang, Z.-Y.; Laskin, J. Nano-DESI Mass Spectrometry Imaging of Proteoforms in Biological Tissues with High Spatial Resolution. *Anal Chem* **2023**, *95* (12), 5214–5222. https://doi.org/10.1021/acs.analchem.2c04795.
- (48) Unsihuay, D.; Hu, H.; Qiu, J.; Latorre-Palomino, A.; Yang, M.; Yue, F.; Yin, R.; Kuang, S.; Laskin, J. Multimodal High-Resolution Nano-DESI MSI and Immunofluorescence

- Imaging Reveal Molecular Signatures of Skeletal Muscle Fiber Types. *Chem Sci* **2023**, *14* (15), 4070–4082. https://doi.org/10.1039/D2SC06020E.
- (49) Weigand, M. R.; Yang, M.; Hu, H.; Zensho, C.; Laskin, J. Enhancement of Lipid Signals with Ammonium Fluoride in Negative Mode Nano-DESI Mass Spectrometry Imaging. *Int J Mass Spectrom* **2022**, *478*. https://doi.org/10.1016/J.IJMS.2022.116859.
- (50) Unsihuay, D.; Qiu, J.; Swaroop, S.; Nagornov, K. O.; Kozhinov, A. N.; Tsybin, Y. O.; Kuang, S.; Laskin, J. Imaging of Triglycerides in Tissues Using Nanospray Desorption Electrospray Ionization (Nano-DESI) Mass Spectrometry. *Int J Mass Spectrom* 2020, 448, 116269. https://doi.org/10.1016/J.IJMS.2019.116269.
- (51) Michelmann, K.; Silveira, J. A.; Ridgeway, M. E.; Park, M. A. Fundamentals of Trapped Ion Mobility Spectrometry. *J Am Soc Mass Spectrom* **2015**, *26* (1), 14–24. https://doi.org/10.1007/s13361-014-0999-4.
- (52) Jeanne Dit Fouque, K.; Ramirez, C. E.; Lewis, R. L.; Koelmel, J. P.; Garrett, T. J.; Yost, R. A.; Fernandez-Lima, F. Effective Liquid Chromatography-Trapped Ion Mobility Spectrometry-Mass Spectrometry Separation of Isomeric Lipid Species. *Anal Chem* 2019, 91 (8), 5021–5027. https://doi.org/10.1021/acs.analchem.8b04979.
- (53) Ridgeway, M. E.; Silveira, J. A.; Meier, J. E.; Park, M. A. Microheterogeneity within Conformational States of Ubiquitin Revealed by High Resolution Trapped Ion Mobility Spectrometry. *Analyst* **2015**, *140* (20), 6964–6972. https://doi.org/10.1039/C5AN00841G.
- (54) Willems, S.; Voytik, E.; Skowronek, P.; Strauss, M. T.; Mann, M. AlphaTims: Indexing Trapped Ion Mobility Spectrometry–TOF Data for Fast and Easy Accession and Visualization. *Molecular & Cellular Proteomics* **2021**, *20*, 100149. https://doi.org/10.1016/J.MCPRO.2021.100149.

TOC:

